CHEMISTRY OF MATERIALS

pubs.acs.org/cm

Article

Reaction Selectivity in Cometathesis: Yttrium Manganese Oxides

Allison Wustrow, Matthew J. McDermott, Daniel O'Nolan, Chia-Hao Liu, Gia Thinh Tran, Brennan C. McBride, Simon M. Vornholt, Chao Feng, Shyam S. Dwaraknath, Karena W. Chapman, Simon J. L. Billinge, Wenhao Sun, Kristin A. Persson, and James R. Neilson*

Cite This: *Chem. Mater.* 2022, 34, 4694−4702

Read Online

ACCESS | Metrics & More | Article Recommendations | Supporting Information

ABSTRACT: Synthesis of metastable materials by control of reaction pathways is facilitated by low-temperature routes. Cometathesis reactions have recently been shown to lower reaction temperatures when compared to single-ion metathesis reactions. Here, we share the discovery of how and why different precursor combinations radically change the reaction pathway and selectively yield different product polymorphs. By studying reactions of the general form, $xA_yMnO_2 + (1 - x)\ A'_zMnO_2 + YOCl \rightarrow YMnO_3 + xA_yCl + (1 - x)A'_zCl$ (A and A′ = Li, Na, Mg, and Ca, y and $z = 1/2$ or 1, and $0 \leq x \leq 1$) using *ex post facto* synchrotron X-ray diffraction, we determine reaction onset temperatures and reaction intermediates for various combinations of A and A′. These observations highlight the importance of the nascent halide salt product in determining the reaction onset temperature, which is lower for all studied cometathesis reactions than the reaction temperatures of the constituent single-ion metathesis reactions. In addition, the spectating alkali and alkaline earth species determine the accessible intermediates, which steers the reaction pathways toward different product phases. While each of the studied cations has a unique reaction pathway, polymorph-selective synthesis is only achieved with a mixture of alkali or alkaline earth cations. Specifically, cation combinations of Li and Na produce phase-pure products of the hexagonal polymorph of $YMnO_3$ and mixtures of Li and Mg or Mg and Ca produce orthorhombic $YMnO_3$. Altogether, this study highlights how chemical potentials at reacting interfaces and the propensity to form defective structures dictates the reaction pathway such that one can target metastable materials by controlling the reaction pathways.

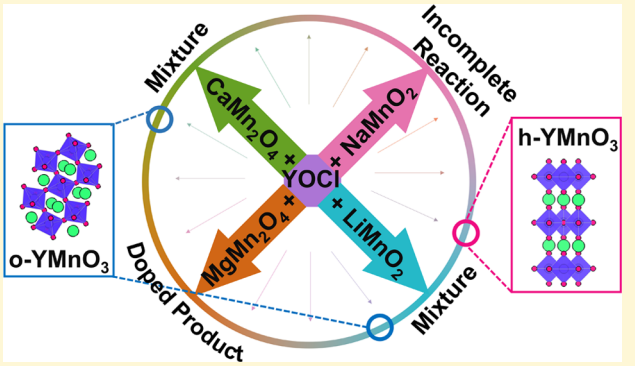

INTRODUCTION

In the synthesis of metastable oxides, lower-temperature reactions (e.g., less than 1000 °C) are often preferred to classic high-temperature solid-state reactions, which promote decomposition into the most stable form. As solid-state reactions tend to be mass-transport limited, solution-based routes improve mobility within a system, allowing for lower-temperature reactions and greater selectivity. For example, a wide range of vanadium oxides can be obtained using hydrothermal synthesis by tuning the reaction pH.[1] Flux synthesis is another frequently used solution-based route to solid materials, with molten salts and other low-melting-point phases acting as the solvent, increasing ionic transport.[2] In the case of a metathesis (double replacement) reaction, such molten halide salt phases can be produced alongside the target product.[3,4] Metathesis reactions are typically considered to be self-propagating if the heat produced by the exothermic reaction is sufficient to melt the produced salt, improving transport in the system and creating a runaway chain reaction.[5] Temperatures in metathesis reactions can reach >1000 °C after ignition.[6] However, recent studies have revealed how low-temperature, non-self-sustaining metathesis reactions can provide access to compounds that become unstable at high temperatures, such as FeS_2,[7] $ZnSnN_2$,[8] or $MgCr_2S_4$.[9] Direct synthesis of these phases via conventional approaches is typically difficult,[10] and metathesis offers a facile route to their production.

Metathesis reaction temperatures are further lowered using cometathesis. In cometathesis reactions, a combination of precursors are used to produce a mixture of salt products (e.g., two alkaline earth ions). The mixture of the salts can have a lower melting point than either salt individually when the salts form a eutectic. It was previously shown that including both $MgMn_2O_4$ and $CaMn_2O_4$ in a reaction with YOCl yields a $Mg_{1-x}Ca_xCl_2$ eutectic along with $YMnO_3$, and the reaction temperature is lowered by 100 °C relative to either reaction individually.[11] At lower reaction temperatures, the nominally

Received: February 28, 2022
Revised: April 26, 2022
Published: May 10, 2022

"spectator" ions (e.g., alkali and alkaline earth) play an important role in dictating the reaction pathway.

The yttrium manganese oxide (Y−Mn−O) chemical system contains several ternary phases with similar formation energies (e.g., $YMnO_3$, YMn_2O_5, and $Y_2Mn_2O_7$); small variations in the synthetic approach lead to notable changes in selectivity for the reaction. For example, reactions of Li_2CO_3, YCl_3, and Mn_2O_3 in flowing O_2 yield phase-pure orthorhombic $YMnO_3$, but replacing the lithium carbonate precursor with Na_2CO_3 leads to $Y_2Mn_2O_7$, and K_2CO_3 leads to a mixture of products.[12] In those reactions, various A_xMnO_2 and YOCl intermediates are observed, and the relative stability of these intermediates and their propensity to form defects hints at their ability to control the reaction pathway.[13,14] Similarly, reactions of $LiMnO_2$,[13,15] $MgMn_2O_4$, or $CaMn_2O_4$[11] with YOCl have unique reaction pathways, which change the selectivity of these reactions.

Here, we observe and explain the reaction onset temperature and product selectivity, or lack thereof, of various cometathesis reactions, which form $YMnO_3$. $YMnO_3$ is traditionally synthesized by a reaction of the two constituent binary oxides requiring temperatures of over 1000 °C, which yields the hexagonal polymorph h-$YMnO_3$.[16] Annealing the binary oxides at temperatures below 850 °C does not produce a single-$YMnO_3$ phase (Figure 1).[17] The high temperatures required

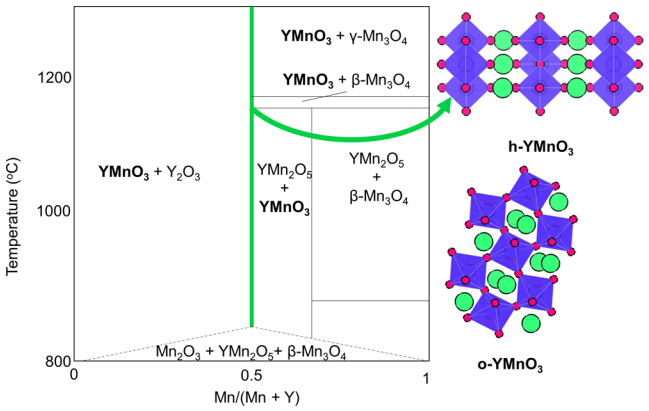

Figure 1. Phase diagram of the Y−Mn−O system.[17] $YMnO_3$ does not form directly from the binaries at temperatures below 850 °C, so indirect reaction routes must be taken to yield o-$YMnO_3$, which is not the thermodynamically stable polymorph at high temperatures.

for the formation of $YMnO_3$ prevent the formation of the orthorhombic polymorph o-$YMnO_3$, which transforms to h-$YMnO_3$ at temperatures above 980 °C.[18] Therefore, to control polymorph selectivity in the $YMnO_3$ system, it is important to control reaction temperatures. To this end, we investigate combinations of Li, Mg, Ca, and Na, and highlight the origin of specificity for each cation. Using a gradient furnace and *ex post facto* synchrotron X-ray diffraction studies, we examine the general reaction $xA_yMnO_2 + (1 - x)\ A'_zMnO_2 + YOCl \rightarrow YMnO_3 + xA_yCl + (1 - x)\ A'_zCl$ (A and A′ = Li, Na, Mg, and Ca, y and z = 1/2 or 1, and $0 \leq x \leq 1$). We show that all combinations of two cations lower the reaction onset temperature compared to single-cation metathesis, consistent with the melting points of the eutectic halide salts. While none of the single-cation metathesis reactions result in a phase-pure $YMnO_3$ product, specific combinations of cation pairs produce phase-pure and polymorph selective powders of both o-$YMnO_3$ and h-$YMnO_3$ through a cometathesis reaction. Finally, we show how the selectivity rules of cometathesis reactions differ from the selectivity rules of the constituent individual cation metathesis reactions, and specifically how balancing reaction pathways, as discussed in previous publications such as through defect accommodation in reaction intermediates[15] and structural templating,[11] allows specific products to be targeted.

METHODS

Precursor Preparation. Precursors were prepared according to previously reported syntheses detailed here. Material purity was confirmed using powder X-ray diffraction (PXRD) collected on a Bruker D8 Discover diffractometer using Cu Kα radiation and a Lynxeye XE-T position-sensitive detector. All experimental methods described below are machine-readable by the "Syncheck" algorithm[19] used to extract recipes in a systematic manner that will allow for deeper analysis in future studies.[20] Graphical representations of syncheck results are shown in Figures S1−S5.

To synthesize YOCl, $YCl_3 \cdot 6H_2O$ was heated to 400 °C for 4 h in air.[21] This reaction releases HCl vapor, and thus should be conducted in a tube furnace; once reacted the resulting white powder was stored in air.

The tetragonal polymorph of $LiMnO_2$ was synthesized in a two-step process.[22] In the first step, Li_2CO_3 and MnO_2 (1:4 molar) were mixed and heated at 800 °C for 12 h in air to form $LiMn_2O_4$. Second, $LiMn_2O_4$ and lithium iodide (1:7 molar ratio) were heated to 80 °C for 2−4 days in acetonitrile under reflux and with constant nitrogen flow. The resulting brown powder was collected by filtration in air. The powder was stored in a glovebox.

Note: The reaction was considered complete when the diffraction pattern contained a single peak around 18.3° using Cu Kα radiation. If both the (111) peak of $LiMn_2O_4$ and the (110) peak of tetragonal $LiMnO_2$ could be observed, fresh LiI was added and the sample and the reflux was continued until all of the $LiMn_2O_4$ had reacted.

For the synthesis of $NaMnO_2$, Na_2CO_3 and MnO_2 (1:2 molar ratio) were ground together and heated to 700 °C for 24 h in air.[23] The product was then quenched directly into a glovebox antechamber, and the material was stored under argon. Unlike $LiMnO_2$ which is stable in air for short periods of time, $NaMnO_2$ should always be handled under an inert atmosphere to avoid oxidation.

$MgMn_2O_4$ was prepared using a sol−gel method.[24] $Mg(NO_3)2\cdot 6H_2O$ and $Mn(NO_3)2\cdot 4H_2O$ (1:2 molar ratio) were dissolved in water with a molar excess of citric acid. The solution was stirred overnight and then heated to 100 °C for 16 h until the water boiled off. The resulting orange foam was transferred to an alumina crucible and heated at 650 °C for 12 h. The product was cooled slowly for 6 h in air. The resulting brown powder can be stored in air.

For $CaMn_2O_4$:$CaCO_3$ and MnO_2 (1:2 molar ratio) were ground together and heated to 980 °C overnight in air.[25] The resulting powder was reground, and heated to 1300 °C for 14 days in air. Every 4 days, the reaction mixture was reground to increase surface area. The resulting dark powder could be stored in air.

Diffraction Experiments. *Ex post facto* (after heating) measurements were run on mixtures of YOCl with one or two of the manganese-containing precursors mentioned above. The relative amount of Mn and Y in the system was kept equivalent between samples. For cometathesis reactions, ratios between the alkali and alkaline earth metals were chosen so that the resulting halide salt would have the lowest melting temperature possible unless otherwise noted. Samples were loaded into a 1.1 mm OD/1.0 mm ID quartz capillary and sealed under argon. Samples were heated using a gradient flow cell furnace[26] for 40 min before being cooled to room temperature. The gradient furnace heats capillaries unevenly in a reproducible manner, and the position along the capillary is correlated to sample temperature. Calibration of the temperature at each sample position in the furnace was performed by heating a capillary of Si and NaCl and determining the temperature of a given point by thermal expansion.[27]

https://doi.org/10.1021/acs.chemmater.2c00636
Chem. Mater. 2022, 34, 4694−4702

Synchrotron diffraction experiments were performed at the 28-ID-2 beamline at the National Synchrotron Light Source II at Brookhaven National Laboratory. Data were collected with X-ray wavelengths of 0.1949 and 0.1939 Å. Data were collected on a PerkinElmer plate detector at a sample-to-detector distance of 1400 mm. The experimental data were reduced in real time using the open-source analysis software xpdAn and xpdTools, which are maintained by the xpdAcq organization on GitHub (https://github.com/xpdAcq).[28] TOPAS v6 was used to analyze the final composition of each metathesis and cometathesis reaction. Reaction onset temperature was determined using a Pearson correlation analysis in the following manner. Each diffraction pattern was compared to a simulated pattern of o-$YMnO_3$ and h-$YMnO_3$ generated using TOPAS using instrumental terms determined by the Rietveld analysis of a single diffraction pattern. As the Pearson method scales linearly, higher Pearson coefficients correspond to a greater amount of the targeted phase within the sample. This method allows quick determination of the temperatures where the targeted $YMnO_3$ phases form in a high-throughput manner.

Thermodynamic Free Energies. Thermodynamic free energies for phases in the Y−Mn−O−Li−Na−Mg−Ca−Cl chemical system were estimated using the same approach as described in a previous work.[29] Atomic structures and their calculated energies were acquired from the Materials Project (MP), a density functional theory (DFT) calculation database (version 2021.11.10).[30] Gibbs free energies of formation, ΔG_f, of solid compounds were estimated using the machine-learned Gibbs free energy descriptor approach implemented by Bartel, et al.[31] and applied to MP data at a temperature of T = 800 °C. For compounds with corresponding experimental references in the NIST-JANAF thermochemical tables (e.g., Li_2O_2, NaCl), the formation energy was interpolated from the reference tables.[32]

Phase Equilibria Calculations. Chemical potential diagrams were constructed via the method described by Todd, et al.[14] and implemented in the pymatgen package.[33] Predominance diagrams were illustrated by viewing the chemical potential diagram's surface from one of the sides so that only two dimensions were visible (Figure 2a−d). The stability domains for the alkali or alkaline earth manganese oxide phases (A_xMnO_2) in μ_Y−μ_{Mn} space were illustrated by plotting a lower-dimensional slice of their stability domain within the full A−Mn−O−Y chemical potential space. This allows for convenient visualization of phase equilibria between the A_xMnO_2 and Y−Mn−O phases, where the A_xMnO_2 domains overlapping with the other phase domains represent shared boundaries, or phase coexistence, in higher-dimensional chemical potential space.

RESULTS AND DISCUSSION

Reactions of the form $xA_yMnO_2 + (1 - x)A'_zMnO_2$ + YOCl (A, A′ = Li, Na, Mg, Ca; $y, z \in [0.5, 1]$) were studied using *ex post facto* powder synchrotron X-ray diffraction. Reagents were chosen to target a $YMnO_3$ final product and corresponding halide salt products. Samples were typically heated on a gradient furnace for 40 min before being cooled to room temperature.[26] Once cooled, diffraction patterns were collected. These diffraction patterns are referred to as *ex post facto* (after the fact) in this manuscript. The collection of data at room temperature allows for meaningful comparisons to be drawn between samples regarding lattice parameters as effects from thermal expansion are negligible.

Single-Ion Metathesis. The A species in the reaction A_xMnO_2 + YOCl (A = Li, Na, Mg, Ca) differentiate the accessible reaction pathways that impart selectivity over the reaction product. Reaction products are summarized in Table 1 and presented in a more complete version in the supporting information (Table S1). Reactions where A = Li, Mg, and Ca have previously been reported in the literature,[11,15] and the previously established results are restated here. In reactions of $LiMnO_2$ with YOCl, a charge disproportionation reaction in the Li−Mn−O intermediates creates two concurrent reaction pathways. As oxidizing the Mn reduces the symmetry of the intermediate (Figure 2e) charge disporportionation in the intermediates is detectable by powder diffraction. Slightly oxidized Li−Mn−O phases lead to o-$YMnO_3$; slightly reduced Li−Mn−O phases lead to h-$YMnO_3$. The two ternary oxides form concurrently at 550 °C. In the reaction of $CaMn_2O_4$ with

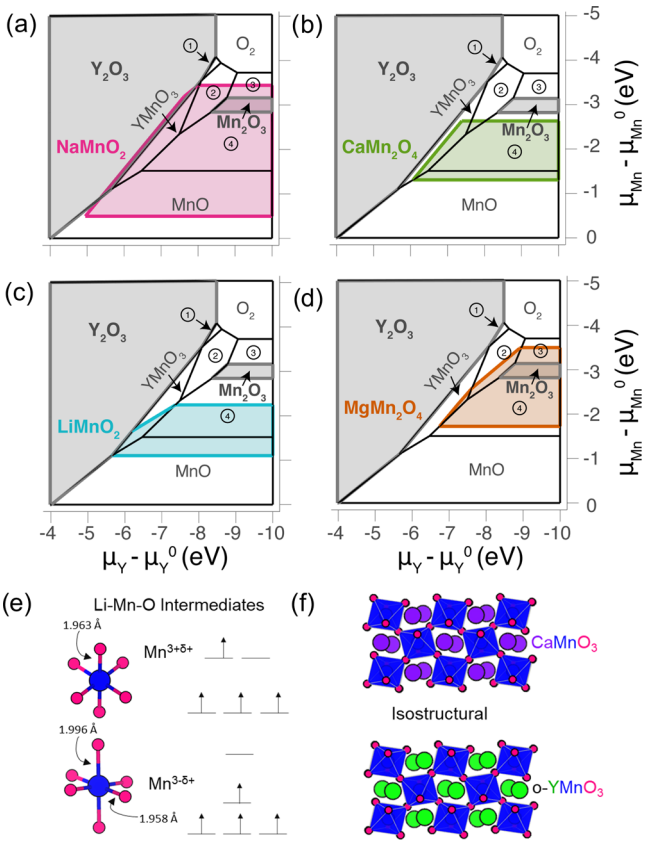

Figure 2. Predominance diagrams of the Y−Mn−O system overlaid with slices of alkali or alkaline earth manganese oxide stability domains. The overlaid slices correspond to the phases (a) $NaMnO_2$, (b) $CaMn_2O_4$, (c) $LiMnO_2$, and (d) $MgMn_2O_4$. Only $NaMnO_2$ overlaps with both Y_2O_3 and Mn_2O_3. The circled numerical labels correspond to the stability domains for the phases: (1) $Y_2Mn_2O_7$, (2) YMn_2O_5, (3) MnO_2, and (4) Mn_3O_4. Polymorph selectivity for $YMnO_3$ phases is determined by accessible intermediates. Reactions of $LiMnO_2$ with YOCl form a mixture of Li−Mn−O intermediates leading to a mixture of $YMnO_3$ products (e),[15] while reactions of $MgMn_2O_4$ and $CaMn_2O_4$ with YOCl yield o-$YMnO_3$ owing to alkaline earth metal substitution (f).[11]

Table 1. Compositions of Final Products of Metathesis Reactions Determined from Rietveld Refinements 50 °C above the Reaction Onset as Determined by the Pearson Correlation Method: Halide Salt Products and Small Amounts of Reactants and Intermediates Are Not Accounted for in This Table[a]

	Li (%)	Na (%)	Mg (%)	Ca (%)
h-$YMnO_3$	60			18
o-$YMnO_3$	40			72
binaries		100		
Mg:o-$YMnO_3$			100	

[a]A more complete summary is found in the Supporting Information (Table S1).

https://doi.org/10.1021/acs.chemmater.2c00636
Chem. Mater. 2022, 34, 4694−4702

YOCl, more o-$YMnO_3$ is produced than h-$YMnO_3$. As $CaMnO_3$ and o-$YMnO_3$ are isostructural (Figure 2f), the remaining Ca in the structure likely templates the orthorhombic structure. However, at the high temperatures required for that reaction to take place (690 °C), the o-$YMnO_3$ converts to h-$YMnO_3$. The hexagonal phase is more thermodynamically stable at higher temperatures if no defects are present.[12,15,34] The reaction of $MgMn_2O_4$ with YOCl also favors o-$YMnO_3$ for similar reasons to $CaMn_2O_4$. Despite the higher reaction temperature with $MgMn_2O_4$ (715 °C), there is no conversion to h-$YMnO_3$. The reaction between $MgMn_2O_4$ and YOCl is only thermodynamically favorable when Mg substitutes into the final $YMnO_3$ product, causing a lattice contraction (Figure S6). This substitution stabilizes the orthorhombic polymorph over the hexagonal polymorph leading to a phase-pure product. The accessible intermediates of reactions containing Li, Mg and Ca all direct the polymorph selectivity of the $YMnO_3$ ternary oxide product.

In contrast, reactions of $NaMnO_2$ with YOCl form binary oxides instead of ternary oxides within the temperature range of this study. After reaction at 775 °C, the final products are a mixture of Y_2O_3, MnO_2, Mn_3O_4, and NaCl with a small amount of Mn_2O_3 present (Figure S7). Although the manganese oxide species charge disproportionates, an overall average oxidation state of Mn^{3+} is maintained. The differences in selectivity can be rationalized by observing where A−Mn−O phases overlap on the Y−Mn−O predominance diagram (Figure 2a−d). $NaMnO_2$ is stable over a wide range of chemical potentials, which has previously been shown to promote the formation of $Y_2Mn_2O_7$ in reactions under flowing oxygen.[14] However, in evacuated systems with a lower oxygen chemical potential, the formation of $Y_2Mn_2O_7$ is not viable. $NaMnO_2$ forms a stable interface with Y_2O_3 as well as all of the relevant manganese oxide phases, as indicated by their overlapping phase fields in the predominance diagrams. In contrast, neither $CaMn_2O_4$ nor $MgMn_2O_4$ overlap with Y_2O_3, and $LiMnO_2$ does not overlap with Mn_2O_3, making direct reaction to form binary oxides from these precursors unfeasible without producing $YMnO_3$ in the process. As observed with the $NaMnO_2$ precursor, the formation of the binary oxides is kinetically favorable over the formation of ternary $YMnO_3$, as the former does not require transport of any of the less mobile trivalent cations in the system. The wide span of chemical potentials over which $NaMnO_2$ is stable leads the precursor to have a more varied chemistry than other similar phases; when excess oxygen is present it provides a direct pathway to $Y_2Mn_2O_7$,[14] but without excess oxygen, the formation of binary oxides over ternary oxides is favored.

Cometathesis Reaction Onset Temperatures. Combining multiple single-ion metathesis reactions in the same vessel results in a cometathesis reaction. A minor extent of reaction forms a nascent halide salt phase, which melts at lower temperatures than either halide salt independently, allowing for faster reaction, more salt formation, and a cascading reaction. We identified the lowest reaction temperature at which $YMnO_3$ forms after 40 min of heating. Reaction onset temperatures are determined by comparing a calculated pattern of both polymorphs of $YMnO_3$ to *ex post facto* PXRD patterns using a Pearson correlation analysis. This statistical method determines if numerical values for two data sets increase and decrease simultaneously, allowing for rapid determination of data sets which do and do not contain the phase of interest. Pearson correlation functions of each polymorph and onset reaction temperatures for each combination of cations are found in the Supporting Information (Figure S8 and Table S2). These methods were used to rapidly identify patterns containing either of the ternary final products of the reaction. In all cases, reaction onset temperatures are lower for the cometathesis system than for either endpoint independently. However, their relationship to the eutectic melting temperature is slightly more complicated. Figure 3 summarizes the onset reaction temperature for the systems studied here.

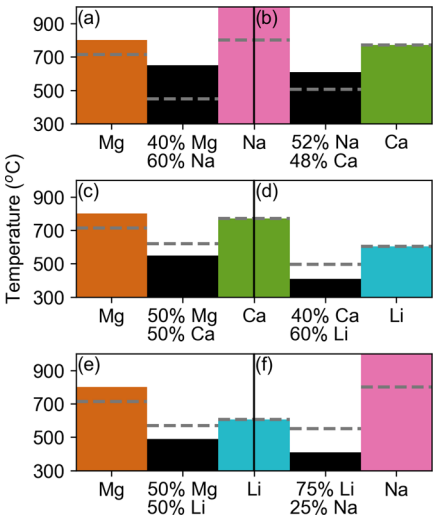

Figure 3. Onset temperature of reaction for cometathesis reactions at the eutectic composition for the relevant halide salts for (a) Mg/Na, (b) Na/Ca, (c) Mg/Ca, (d) Ca/Li, (e) Mg/Li, and (f) Li/Na. T_{rxn} as determined from the Pearson correlation is shown in black, surrounded by T_{rxn} of the single-ion metathesis reactions for comparison. The melting point of the representative halide salt is indicated by a dashed gray line in each system.

The cometathesis systems of Mg−Ca, Mg−Li, and Li−Ca react roughly 50 °C below the melting point of their resulting eutectic salt mixtures. While the solvation of Y, Mn, and O into the eutectic chloride mixture could conceivably further depress the melting point of the halide salt, the observation of crystalline halide salts by diffraction dictates that bulk melting is not necessary to obtain enhanced reactivity, consistent with our prior observations.[11] Instead, this lowering in temperature is attributed to surface melting of the halide salt product. Surface melting, sometimes called pre-melting, is to the solid/liquid transition as vapor pressure is to the liquid/gas transition. As the melting point of the solid is approached, a quasi-liquid layer is formed on the surface of the solid, which is more disordered than the solid phase, yet more ordered than the liquid phase.[35] At the earliest stages of the metathesis reaction, nascent salt crystals form. As the temperature of the system approaches the melting point, the quasi-liquid layer promotes transportation within the reaction system, allowing for the formation of ternary oxides as well as the production of more halide salt in an autocatalytic manner (Figure 4).

The cometathesis reaction between $CaMn_2O_4$, $MgMn_2O_4$, and YOCl is described in detail in a previous work[11] and is summarized here. o-$YMnO_3$ forms at 550 °C, 50 °C below the eutectic melting point of a mixture of $MgCl_2$ and $CaCl_2$. The initial melting point of the $MgCl_2$−$CaCl_2$ system is composition independent in systems with >20 mol % Mg,

https://doi.org/10.1021/acs.chemmater.2c00636
Chem. Mater. 2022, 34, 4694−4702

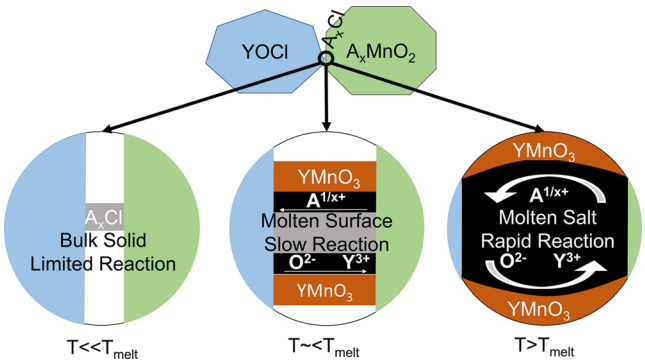

Figure 4. Schematic of surface melting in a reaction. As the temperature approaches the melting point of the salt (gray), a quasi-liquid layer forms at the surface (black), creating a conduction path for reactive species and allowing for the accelerated formation of $YMnO_3$ (orange). The thickness of this layer increases until the melting point is reached, at which point bulk melting occurs.

and as such, the onset temperature of reaction is also independent of composition. Similarly, cometathesis reactions of $LiMnO_2$ and $MgMn_2O_4$ with YOCl have temperature onsets around 50 °C below the eutectic melting temperature. Unlike the Ca−Mg system, the melting onset temperature of a mixture of LiCl and $MgCl_2$ varies between 565 and 615 °C. The reaction onset temperature for reactions of the form $(1-x)LiMnO_2 + x\ MgMn_2O_4 + (1+x)$ YOCl follow the shape of the halide salt phase diagram, again roughly 50 °C below the expected melting point (Figure 5). Reactions of $CaMn_2O_4$,

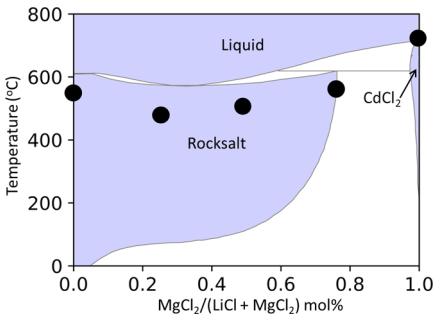

Figure 5. Onset temperature of reaction for cometathesis reactions in the Mg/Li system overlaid on the binary phase diagram of LiCl and $MgCl_2$.

$LiMnO_2$, and YOCl also begin forming $YMnO_3$ roughly 50 °C below the eutectic melting point of a LiCl−$CaCl_2$ mixture. Cometathesis reactions for the three non-Na-containing systems are mediated by surface melting of the produced halide salt.

In cometathesis reactions between Na and alkaline earth metal precursors, the reaction onset temperature is *above* the melting point of the eutectic salt. While the eutectic melting point of NaCl with $MgCl_2$ and $CaCl_2$ is 450 and 500 °C, respectively, formation of $YMnO_3$ is not seen until 610 °C in the Na/Ca system and 670 °C in the Na/Mg system. Reaction onsets are more gradual than in the Mg/Li and Ca/Mg systems, with reactions reaching completion at 100 °C above the onset temperatures. It is difficult to directly compare reaction onset temperatures of cometathesis reactions with reactions of $NaMnO_2$ and YOCl, as the reactions yield different products. However, as Mn_2O_3 and Y_2O_3 react to form $YMnO_3$ at 1300 °C, it is reasonable to assume that a reaction of $NaMnO_2$ and YOCl eventually forms $YMnO_3$, but that the reaction requires higher temperatures than were used in this study. In cometathesis reactions between alkaline earth manganese oxides, $NaMnO_2$, and YOCl, reaction onset was seen around 100 °C below the onset reaction temperature for the alkaline earth manganese oxide reactions. In the case of Na/Li cometathesis, the reaction occurs around 150 °C lower than reactions of only $LiMnO_2$ with YOCl, significantly below the LiCl/NaCl eutectic melting point.

The different behavior of Na-containing cometathesis reaction temperatures is consistent with the difference in surface melting between NaCl and other halide salts. While surface melting occurs in a wide range of species such as DNA,[36] water,[37] and oxides,[38] the effect is not universal. Instead, the ability of the melt to wet the surface of the corresponding solid determines the surface melting character of a phase.[39] NaCl is known to have particularly poor surface wetting, with a contact angle between the melt and the solid of 48.1°.[40] LiCl by comparison has a contact angle of 32.3°, indicating that the isostructural salt will exhibit a greater degree of surface melting.[41] Solid solutions of NaCl and LiCl have also been shown to exhibit greater surface wetting than the parent halides,[41] which accounts for the lower reaction temperature seen in Na−Li cometathesis. Measurements performed on molten $MgCl_2$ and $CaCl_2$ mention that the molten salts easily wet surfaces,[42] and indeed the data collected in this work is consistent with the mixtures of $CaCl_2$, $MgCl_2$, and LiCl surface melting around 50 °C below the reported melting point. We propose that a lack of surface melting in NaCl does not allow for easy transport of ions within the system, and it also limits the formation of chloride salt mixtures containing two cations. This in turn prevents the melting point depression that would be expected from a eutectic mixture. Both the $MgCl_2$−NaCl and $CaCl_2$−NaCl eutectics have significantly depressed melting points, so temperatures exist which are both significantly above the melting point of the halide salt and below the reaction onset for either Ca or Mg single-ion metathesis. It is in this region that the onset temperatures for Mg−Na and Ca−Na cometathesis occur, roughly 100 °C below the onset temperature for the single-ion metathesis. We propose that at these elevated temperatures, small amounts of Na are able to dissolve into the alkaline earth halides, depressing the melting point and allowing for a lowering of the onset reaction temperature. However, the melting point of the salt mixture is too cold to allow this mixing to take place, preventing reaction at the melting point of the eutectic salt.

Final Reaction Products in Cometathesis Reactions. Final products of cometathesis reactions include o-$YMnO_3$, h-$YMnO_3$, Mg-substituted o-$YMnO_3$, small amounts of binary oxides, and mixtures of these phases. While amorphous phases are likely present after only 40 min of reaction, the diffraction data provide insight into product selectivity. To determine this selectivity in cometathesis reactions, diffraction patterns corresponding to ca. 50 °C above reaction onset for each composition are fit using product phases (Figure S9). A numeric summary of the results is presented in Table 2, and a more complete table is provided in the supporting information (Table S1). Mg-containing reactions are also fit with a second o-$YMnO_3$ phase to capture any of the magnesium substituted yttrium manganese oxide seen previously in Mg cometathesis reactions (Figure S6). Note that while cometathesis reactions

https://doi.org/10.1021/acs.chemmater.2c00636
Chem. Mater. 2022, 34, 4694−4702

Table 2. Compositions of Final Products of Cometathesis Reactions Determined from Rietveld Refinements 50 °C above the Reaction Onset as Determined from the Pearson Method[a]

	75% Li 25% Na	50% Li 50% Na	25% Li 75% Na
h-$YMnO_3$	100%	83%	81%
o-$YMnO_3$		3%	6%
binaries		14%	13%
	75% Li 25% Mg	50% Li 50% Mg	25% Li 75% Mg
h-$YMnO_3$		3%	
o-$YMnO_3$	99%	36%	28%
binaries	1%	2%	
Mg:o-$YMnO_3$		58 %	72%
	75% Ca 25% Mg	50% Ca 50% Mg	25% Ca 75% Mg
h-$YMnO_3$		3 %	
o-$YMnO_3$	100%	58%	12%
binaries			
Mg:o-$YMnO_3$		58%	88%
	60% Na 40% Mg	52% Na 48% Ca	40% Ca 60% Li
h-$YMnO_3$	69%	45%	43%
o-$YMnO_3$		54%	56%
binaries	1%	1%	1%
Mg:o-$YMnO_3$	30%		

[a]Halide salt products and small amounts of reactants and intermediates are not shown.

go to >90 % completion with respect to crystalline phases, single-ion alkaline earth reactions only convert <20 % to yttrium manganese oxide phases while heated to 750 °C for 2 h. Figure 6 and Table 2 show the distribution of final products in the reaction at 50 °C above the reaction onset, excluding the relevant chloride salts as well as remaining reactants and intermediates present in the single metathesis systems. In Li−Mg and Ca−Mg systems, phase-pure o-$YMnO_3$ is formed in Mg-poor compositions, and phase-pure h-$YMnO_3$ is formed in Li-rich Li−Na systems.

The A−Mn−O intermediates available in a given reaction direct the selectivity of the final reaction loosely following trends imparted by the single-ion reactions. h-$YMnO_3$ and o-$YMnO_3$ polymorphs are very close in energy. At high temperatures (T = 1200 °C), h-$YMnO_3$ is more stable,[34] but small amounts of Mn oxidation cause the orthorhombic polymorph to be more stable than the hexagonal polymorph; indirect evidence suggests that near-stoichiometric o-$YMnO_3$ could become more stable than h-$YMnO_3$ below ca. 550 °C.[13] In Li single-ion metathesis, two Li−Mn−O intermediates form: one of the intermediates is more oxidized, the other more reduced, and this charge disproportionation leads to a mixture of $YMnO_3$ polymorphs in the final product, with h-$YMnO_3$ being more prevalent than o-$YMnO_3$.[15] In Ca single-ion metathesis, Ca ions template the orthorhombic $YMnO_3$ structure, which is isostructural with $CaMnO_3$.[11] The product of a Li−Ca cometathesis reaction is a mixture of both $YMnO_3$ polymorphs: it produces more h-$YMnO_3$ than a reaction with pure $LiMnO_2$, and more o-$YMnO_3$ than a reaction with pure $CaMn_2O_4$. Li and Ca affect cometathesis products in a manner consistent with the single metathesis ion products.

While the reaction of $MgMn_2O_4$ with YOCl yields Mg-substituted o-$YMnO_3$, Mg cometathesis reactions yield unsubstituted $YMnO_3$ in Li- and Ca-rich cometathesis reactions. From a theoretical perspective, the reaction between $MgMn_2O_4$ and YOCl to form $YMnO_3$ and $MgCl_2$ has a positive ΔG_{rxn} at the temperatures investigated in this study and therefore should not spontaneously occur.[11] However,

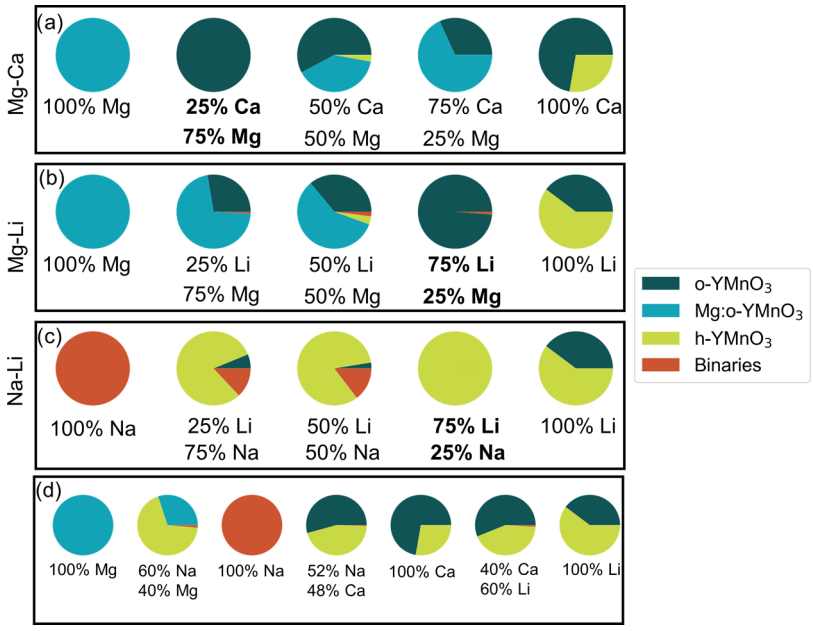

Figure 6. Phase fractions of products from cometathesis reactions between (a) $MgMn_2O_4$ and $CaMn_2O_4$, (b) $LiMnO_2$ and $MgMn_2O_4$, and (c) $NaMnO_2$ and $LiMnO_2$ at the noted composition. (d) Results from additional cometathesis reactions at the eutectic composition of the resulting halide salt are also displayed. o-$YMnO_3$ is shown in dark blue, Mg-substituted $YMnO_3$ in teal, h-$YMnO_3$ in green, and yttrium and manganese oxide binaries in orange. Products were determined from diffraction patterns collected from reaction temperatures approximately 50 °C above the reaction onset, when product formation had ceased as a function of temperature. Composition is reported by weight percent. Compositions resulting in a phase-pure product are shown in bold.

https://doi.org/10.1021/acs.chemmater.2c00636
Chem. Mater. 2022, 34, 4694−4702

those calculations do not consider the thermodynamic favorability of Mg substituting into $YMnO_3$, which is what is experimentally observed. Mg substitution in o-$YMnO_3$ is detectable by a significant contraction of the unit cell and corresponding shifting of peaks in diffraction patterns, as illustrated in Figure S6. Figure 6a,c,d displays significant amounts of the Mg-substituted o-$YMnO_3$ in Mg-rich systems. At a higher Mg concentration in the Mg−Li system, two o-$YMnO_3$ phases are observed, with the phase with the smaller unit cell having Mg substitution. Mg-substituted o-$YMnO_3$ has a smaller unit cell volume in the sample that contained 75% Mg than in the sample which contained 50% Mg (224.4 vs 224.9 $Å^3$) indicating a greater degree of Mg substitution in the final $YMnO_3$ product in systems with more Mg. However, in the reaction with 75% Li and 25% Mg, no evidence of Mg substitution of $YMnO_3$ in the system is observed. In Li-rich regions of the $MgCl_2$−LiCl phase diagrams, instead of forming $CdCl_2$ structured $MgCl_2$, Mg^{2+} dissolves into the LiCl rocksalt structure and no $MgCl_2$ is seen in the final pattern. This dissolution makes it energetically favored for magnesium ions to leave the $YMnO_3$ structure, allowing for unsubstituted $YMnO_3$ to form. These results are consistent with the patterns observed in the previously reported Ca−Mg system.

Reactions of $NaMnO_2$ with YOCl yield a mixture of binary oxides, yet all Na-containing cometathesis reactions have $YMnO_3$ as a major product. While small amounts of binary oxides are produced in sodium-rich reactions in the Na−Li system, the major product of each Na cometathesis reaction studied is one of the polymorphs of $YMnO_3$. Na cometathesis reactions form ternary oxides as the molten halide salts in cometathesis provide a medium for transporting trivalent ions, which is not available in Na single-ion metathesis reactions until temperatures in excess of 800 °C. Na-based cometathesis reactions favor h-$YMnO_3$ over o-$YMnO_3$. The hexagonal polymorph of $YMnO_3$ is more thermodynamically stable than the orthorhombic polymorph at elevated temperatures. Unlike Mg, Li, and Ca systems, Na metathesis systems do not favor the orthorhombic polymorph over the hexagonal polymorph, and thus when the reaction reacts to completion, the more stable h-$YMnO_3$ is favored. Phase-pure h-$YMnO_3$ was formed in reactions which contained 75% $LiMnO_2$ and 25% $NaMnO_2$ as the starting manganese-containing reagent.

CONCLUSIONS

The rich chemistry of cometathesis allows tremendous selectivity in solid-state reactions. Reactions of $LiMnO_2$, $CaMn_2O_4$, $MgMn_2O_4$, and $NaMnO_2$ independently with YOCl do not lead to phase-pure polymorph-selective synthesis of $YMnO_3$; however, cometathesis reactions combinations of Mg−Li and Mg−Ca lead selectively to o-$YMnO_3$, and Li-rich Na−Li cometathesis reactions selectively to h-$YMnO_3$. This selectivity is enabled by both the lower cometathesis reaction temperature and the unique reaction pathways accessible to different alkali and alkaline earth metals. Alkali and alkaline earth metals determine the accessible intermediates and thus reaction processes. In understanding their role, we discovered design rules for targeting specific phases using metathesis. The chemical tunability of metathesis reactions creates reaction outcomes that are more than a sum of their parts.

ASSOCIATED CONTENT

Supporting Information

The Supporting Information is available free of charge at https://pubs.acs.org/doi/10.1021/acs.chemmater.2c00636.

SynCheck flowcharts for all precursor syntheses; example diffraction patterns and their respective refinements; and full summary of products found in diffraction experiments and reaction onset temperatures (PDF)

AUTHOR INFORMATION

Corresponding Author

James R. Neilson − *Department of Chemistry, Colorado State University, Fort Collins, Colorado 80523-1872, United States;* orcid.org/0000-0001-9282-5752; Email: james.neilson@colostate.edu

Authors

Allison Wustrow − *Department of Chemistry, Colorado State University, Fort Collins, Colorado 80523-1872, United States;* orcid.org/0000-0003-1036-9912

Matthew J. McDermott − *Materials Sciences Division, Lawrence Berkeley National Laboratory, Berkeley, California 94720, United States; Department of Materials Science and Engineering, University of California, Berkeley, California 94720, United States;* orcid.org/0000-0002-4071-3000

Daniel O'Nolan − *Department of Chemistry, Stony Brook University, Stony Brook, New York 11790-3400, United States*

Chia-Hao Liu − *Department of Applied Physics and Applied Mathematics, Columbia University, New York, New York 10027, United States*

Gia Thinh Tran − *Department of Chemistry, Colorado State University, Fort Collins, Colorado 80523-1872, United States;* orcid.org/0000-0002-3369-7321

Brennan C. McBride − *Department of Chemistry, Colorado State University, Fort Collins, Colorado 80523-1872, United States;* orcid.org/0000-0002-3825-6138

Simon M. Vornholt − *Department of Chemistry, Stony Brook University, Stony Brook, New York 11790-3400, United States;* orcid.org/0000-0001-9490-3785

Chao Feng − *Department of Materials Science and Engineering, University of Michigan, Ann Arbor, Michigan 48109, United States*

Shyam S. Dwaraknath − *Materials Sciences Division, Lawrence Berkeley National Laboratory, Berkeley, California 94720, United States;* orcid.org/0000-0003-0289-2607

Karena W. Chapman − *Department of Chemistry, Stony Brook University, Stony Brook, New York 11790-3400, United States;* orcid.org/0000-0002-8725-5633

Simon J. L. Billinge − *Department of Applied Physics and Applied Mathematics, Columbia University, New York, New York 10027, United States; Condensed Matter Physics and Materials Science Department, Brookhaven National Laboratory, Upton, New York 11973, United States;* orcid.org/0000-0002-9734-4998

Wenhao Sun − *Department of Materials Science and Engineering, University of Michigan, Ann Arbor, Michigan 48109, United States*

Kristin A. Persson − *Department of Materials Science and Engineering, University of California, Berkeley, California 94720, United States; Molecular Foundry, Lawrence Berkeley*

National Laboratory, Berkeley, California 94720, United States; orcid.org/0000-0003-2495-5509

Complete contact information is available at: https://pubs.acs.org/10.1021/acs.chemmater.2c00636

Notes

The authors declare no competing financial interest.

■ ACKNOWLEDGMENTS

This work was supported as part of GENESIS: A Next Generation Synthesis Center, an Energy Frontier Research Center funded by the U.S. Department of Energy, Office of Science, Basic Energy Sciences under Award Number DE-SC0019212. This research used the 28-ID-1 beamline of the National Synchrotron Light Source II, a U.S. Department of Energy (DOE) Office of Science User Facility operated for the DOE Office of Science by Brookhaven National Laboratory under Contract No. DE-SC0012704. It also made use of the Analytical Resources Core at Colorado State University (SCR_021758).

■ REFERENCES

(1) Chirayil, T.; Zavalij, P. Y.; Whittingham, M. S. Hydrothermal synthesis of vanadium oxides. *Chem. Mater.* **1998**, *10*, 2629−2640.
(2) Bugaris, D. E.; zur Loye, H.-C. Materials discovery by flux crystal growth: quaternary and higher order oxides. *Angew. Chem., Int. Ed.* **2012**, *51*, 3780−3811.
(3) Parkin, I.; Kafizas, A. Exothermic Metathesis Reactions. In *Comprehensive Inorganic Chemistry II*; Elsevier, 2013; pp 471−490.
(4) Wiley, J. B.; Kaner, R. B. Rapid solid-state precursor synthesis of materials. *Science* **1992**, *255*, 1093−1097.
(5) Janes, R. A.; Low, M. A.; Kaner, R. B. Rapid solid-state metathesis routes to aluminum nitride. *Inorg. Chem.* **2003**, *42*, 2714−2719.
(6) Gillan, E. G.; Kaner, R. B. Synthesis of refractory ceramics via rapid metathesis reactions between solid-state precursors. *Chem. Mater.* **1996**, *8*, 333−343.
(7) Martinolich, A. J.; Neilson, J. R. Pyrite formation via kinetic intermediates through low-temperature solid-state metathesis. *J. Am. Chem. Soc.* **2014**, *136*, 15654−15659.
(8) Kawamura, F.; Yamada, N.; Imai, M.; Taniguchi, T. Synthesis of ZnSnN2 crystals via a high-pressure metathesis reaction. *Cryst. Res. Technol.* **2016**, *51*, 220−224.
(9) Miura, A.; Ito, H.; Bartel, C. J.; Sun, W.; Rosero-Navarro, N. C.; Tadanaga, K.; Nakata, H.; Maeda, K.; Ceder, G. Selective metathesis synthesis of MgCr2S4 by control of thermodynamic driving forces. *Mater. Horiz.* **2020**, *7*, 1310−1316.
(10) Wustrow, A.; Key, B.; Phillips, P. J.; Sa, N.; Lipton, A. S.; Klie, R. F.; Vaughey, J. T.; Poeppelmeier, K. R. Synthesis and characterization of MgCr2S4 thiospinel as a potential magnesium cathode. *Inorg. Chem.* **2018**, *57*, 8634−8638.
(11) Wustrow, A.; Huang, G.; McDermott, M. J.; O'Nolan, D.; Liu, C.-H.; Tran, G. T.; McBride, B. C.; Dwaraknath, S. S.; Chapman, K. W.; Billinge, S. J.; et al. Lowering Ternary Oxide Synthesis Temperatures by Solid-State Cometathesis Reactions. *Chem. Mater.* **2021**, *33*, 3692−3701.
(12) Todd, P. K.; Neilson, J. R. Selective formation of yttrium manganese oxides through kinetically competent assisted metathesis reactions. *J. Am. Chem. Soc.* **2019**, *141*, 1191−1195.
(13) Todd, P. K.; Smith, A. M.; Neilson, J. R. Yttrium manganese oxide phase stability and selectivity using lithium carbonate assisted metathesis reactions. *Inorg. Chem.* **2019**, *58*, 15166−15174.
(14) Todd, P. K.; McDermott, M. J.; Rom, C. L.; Corrao, A. A.; Denney, J. J.; Dwaraknath, S. S.; Khalifah, P. G.; Persson, K. A.; Neilson, J. R. Selectivity in Yttrium Manganese Oxide Synthesis via Local Chemical Potentials in Hyperdimensional Phase Space. *J. Am. Chem. Soc.* **2021**, *143*, 15185−15194.
(15) Todd, P. K.; Wustrow, A.; McAuliffe, R. D.; et al. Defect-Accommodating Intermediates Yield Selective Low-Temperature Synthesis of YMnO3 Polymorphs. *Inorg. Chem.* **2020**, *59*, 13639−13650. PMID: 32866379.
(16) Muñoz, A.; Alonso, J.; Martinez-Lope, M.; Casais, M.; Martinez, J.; Fernandez-Diaz, M. Magnetic structure of hexagonal R MnO 3 (R= Y, Sc): Thermal evolution from neutron powder diffraction data. *Phys. Rev. B: Condens. Matter Mater. Phys.* **2000**, *62*, 9498.
(17) Balakirev, V. F.; Vedmid, L.; Yankin, A.; Fedorova, O.; Golikov, Y. V. Heterogeneous phase equilibria in the Tb-Mn-O system. *Inorg. Mater.* **2006**, *42*, 1230−1235.
(18) Moure, A.; Hungría, T.; Castro, A.; Galy, J.; Peña, O.; Tartaj, J.; Moure, C. Doping influence on the stability of YMnO3 orthorhombic perovskite obtained by mechanosynthesis. *Mater. Chem. Phys.* **2012**, *133*, 764−771.
(19) SYNCheck. http://https://www.syncheck.org (accessed Jan 20, 2022).
(20) Konova, O.; Vornholt, S. M.; Rakita, Y.; Billinge, S. J. L.; Parise, J. B.; Ceder, G.; Chapman, K. W. Composing machine-learning compatible synthesis procedures with SynCheck: Best practices and guiding tools *Chem. Mater.*, Submitted.
(21) Wendlandt, W. W. The thermal decomposition of yttrium, scandium, and some rare-earth chloride hydrates. *J. Inorg. Nucl. Chem.* **1957**, *5*, 118−122.
(22) Tarascon, J. M.; Guyomard, D. Li Metal-Free Rechargeable Batteries Based on Li1+ x Mn2 O 4 Cathodes (0 ≤ x ≤ 1) and Carbon Anodes. *J. Electrochem. Soc.* **1991**, *138*, 2864.
(23) Fuchs, B.; Kemmler-Sack, S. Synthesis of LiMnO2 and LiFeO2 in molten Li halides. *Solid State Ionics* **1994**, *68*, 279−285.
(24) Truong, Q. D.; Kobayashi, H.; Nayuki, K.; Sasaki, Y.; Honma, I. Atomic-scale observation of phase transition of MgMn2O4 cubic spinel upon the charging in Mg-ion battery. *Solid State Ionics* **2020**, *344*, No. 115136.
(25) Ling, C. D.; Neumeier, J.; Argyriou, D. N. Observation of antiferromagnetism in Marokite CaMn2O4. *J. Solid State Chem.* **2001**, *160*, 167−173.
(26) O'Nolan, D.; Huang, G.; Kamm, G. E.; Grenier, A.; Liu, C.-H.; Todd, P. K.; Wustrow, A.; Thinh Tran, G.; Montiel, D.; Neilson, J. R.; et al. A thermal-gradient approach to variabletemperature measurements resolved in space. *J. Appl. Crystallogr.* **2020**, *53*, 662−670.
(27) Pathak, P. D.; Vasavada, N. Thermal expansion of NaCl, KCl and CsBr by X-ray diffraction and the law of corresponding states. *Acta Crystallogr., Sect. A: Cryst. Phys., Diffr., Theor. Gen. Crystallogr.* **1970**, *26*, 655−658.
(28) Wright, C. J. Towards Real Time Characterization of Grain Growth from the Melt. Ph.D. Thesis; Columbia University, 2020.
(29) McDermott, M. J.; Dwaraknath, S. S.; Persson, K. A. A graph-based network for predicting chemical reaction pathways in solid-state materials synthesis. *Nat. Commun.* **2021**, *12*, No. 3097. Number: 1 Publisher: Nature Publishing Group.
(30) Jain, A.; Ong, S. P.; Hautier, G.; Chen, W.; Richards, W. D.; Dacek, S.; Cholia, S.; Gunter, D.; Skinner, D.; Ceder, G.; Persson, K. A. Commentary: The materials project: A materials genome approach to accelerating materials innovation. *APL Mater.* **2013**, *1*, No. 011002.
(31) Bartel, C. J.; Millican, S. L.; Deml, A. M.; Rumptz, J. R.; Tumas, W.; Weimer, A. W.; Lany, S.; Stevanović, V.; Musgrave, C. B.; Holder, A. M. Physical descriptor for the Gibbs energy of inorganic crystalline solids and temperature-dependent materials chemistry. *Nat. Commun.* **2018**, *9*, No. 4168.
(32) Malcolm, W.; Chase, J. *NIST-JANAF Thermochemical Tables*, 4th ed.; American Chemical Society; New York: American Institute of Physics for the National Institute of Standards and Technology: Washington, DC, 1998.
(33) Ong, S. P.; Richards, W. D.; Jain, A.; Hautier, G.; Kocher, M.; Cholia, S.; Gunter, D.; Chevrier, V. L.; Persson, K. A.; Ceder, G. Python Materials Genomics (pymatgen): A robust, open-source

python library for materials analysis. *Comput. Mater. Sci.* **2013**, *68*, 314−319.
(34) Kamata, K.; Nakajima, T.; Nakamura, T. Thermogravimetric study of rare earth manganites AMnO3 (A= Sm, Dy, Y, Er, Yb) at 1200° C. *Mater. Res. Bull.* **1979**, *14*, 1007−1012.
(35) Lipowsky, R. Critical surface phenomena at first-order bulk transitions. *Phys. Rev. Lett.* **1982**, *49*, 1575.
(36) Zhou, Y.; Vitkup, D.; Karplus, M. Native proteins are surface-molten solids: application of the Lindemann criterion for the solid versus liquid state. *J. Mol. Biol.* **1999**, *285*, 1371−1375.
(37) Makkonen, L. Surface melting of ice. *J. Phys. Chem. B* **1997**, *101*, 6196−6200.
(38) Marks, L.; Chiaramonti, A.; Rahman, S.; Castell, M. Transition from order to configurational disorder for surface reconstructions on $SrTiO_3$ (111). *Phys. Rev. Lett.* **2015**, *114*, No. 226101.
(39) Di Tolla, F. D.; Ercolessi, F.; Tosatti, E. Maximum overheating and partial wetting of nonmelting solid surfaces. *Phys. Rev. Lett.* **1995**, *74*, 3201.
(40) Grange, G.; Mutaftschiev, B. Méthode de mesure de l'angle de contact à l'interface cristal-bain fondu. *Surf. Sci.* **1975**, *47*, 723−728.
(41) Dupuis, M. M.; Grange, G.; Mutaftschiev, B. Observation of NaCl-LiCl high-temperature phases by gold decoration on the solid—melt interface of czochralski grown crystals. *Phys. Status Solidi A* **1979**, *55*, 385−394.
(42) Sato, Y.; Kuroda, Y.; Nagatsu, T.; Hoshi, M.; Kim, J.-I.; Yamamura, T. Density and Electrical Conductivity of Molten MgCl2-CaCl2 Binary Melt. *ECS Proc. Vol.* **1999**, *1999-41*, No. 313.

https://doi.org/10.1021/acs.chemmater.2c00636
Chem. Mater. 2022, 34, 4694−4702